Polymer 51 (2010) 4375–4382

Contents lists available at ScienceDirect

Polymer

journal homepage: www.elsevier.com/locate/polymer

Microstructural organization of polydimethylsiloxane soft segment polyurethanes derived from a single macrodiol

Taeyi Choi [a], Jadwiga Weksler [b], Ajay Padsalgikar [b], James Runt [a,*]

[a] Department of Materials Science and Engineering, The Pennsylvania State University, University Park, PA 16802, USA
[b] AorTech Biomaterials, Dalmore Drive, Caribbean Park, Scoresby, VIC 3179, Australia

ARTICLE INFO

Article history:
Received 17 May 2010
Received in revised form
20 July 2010
Accepted 21 July 2010
Available online 30 July 2010

Keywords:
Polyurethanes
Polydimethylsiloxanes
Phase separation

ABSTRACT

Segmented polyurethane (PU) block copolymers were synthesized using 4,4′-methylenediphenyl diisocyanate and 1,4-butanediol as hard segments and oligomeric ethoxypropyl polydimethylsiloxane (PDMS) as the soft segments, with hard segment contents ranging from 26 to 52 wt%. The microphase separated morphology, phase transitions, and degrees of phase separation of these novel copolymers were investigated using a variety of experimental methods. Like similar copolymers with mixed ethoxypropyl PDMS/poly(hexamethylene oxide) soft segments, PU copolymers containing only ethoxypropyl PDMS soft segments were found to consist of three microphases: a PDMS matrix phase, hard domains, and a mixed phase containing ethoxypropyl end group segments and dissolved short hard segments. Analysis of unlike segment demixing using small-angle X-ray scattering demonstrates that degrees of phase separation increase significantly as copolymer hard segment content increases, in keeping with findings from Fourier transform infrared spectroscopy measurements.

1. Introduction

It has long been known that poly(dimethylsiloxane) (PDMS) elastomers exhibit outstanding biocompatibility and biostability, but display mechanical properties that are unsuitable for many medical device applications [1–3]. On the other hand, segmented polyurethane (PU) and poly(urethane urea) copolymers have been widely used as mechanically robust elastomers, but typical polyether and polyester soft segment chemistries are susceptible to oxidative and/or hydrolytic degradation *in vivo*, particularly in components involved in longer term implants [4–7]. Early attempts at incorporating PDMS soft segments in PUs, to combine desirable mechanical performance (arising from hard segment microphase separation) with the biostability and biocompatibility of PDMS, did not meet with success due to the difficulty in synthesizing acceptably high molecular PU copolymers from a mixture of polar and non-polar monomers [8–12]. However, significant advances have been made in the past 10 years, with the discovery that high molecular weight (predominately) PDMS soft segments [α,ω-bis(6-hydroxyethoxypropyl) PDMS] could be incorporated into segmented polyurethane copolymers along with a relatively small amount of a second polyether comonomer [poly (hexamethylene oxide), typically 20% of the total soft segment], creating a family of segmented PUs with excellent and tunable mechanical properties that have shown great promise in blood-contacting biomedical applications [13–21]. In a broad sense, the PHMO enhances the "compatibility" between hard segments containing polar urethane moieties and the non-polar siloxane soft segments.

These ethoxypropyl PDMS/PHMO soft segment copolymers, having 4,4′-methylenediphenyl diisocyanate (MDI) and 1,4-butanediol (BDO) as the hard segments, have been found to exhibit a unique three phase microstructure: a PDMS matrix phase, hard domains composed of hard segments, and a mixed phase containing the ether end group segments (ethoxypropyl) of the macrodiol, PHMO, and some dissolved hard segments [19,20]. The mixed phase serves to 'compatibilize' the non-polar PDMS and the dispersed polar hard domains.

To further enhance the biostability of PUs derived from the α,ω-bis (6-hydroxyethoxypropyl) PDMS macrodiol, reduction of PHMO in the soft segment mixture is desirable. Recently [22], a synthetic procedure (summarized in the experimental section) was uncovered that leads to high molecular weight MDI–BDO hard segment PUs using only α,ω-bis(6-hydroxyethoxypropyl) PDMS macrodiol in the reaction. In an early report on these copolymers, we demonstrated that the *in vitro* oxidative biostability was outstanding compared to segmented PUs with other soft segment chemistries under consideration for blood-contacting applications [23]. The phase-separated microstructure and morphology of PUs derived solely from the α,ω-bis(6-hydroxyethoxypropyl) PDMS macrodiol have not however been investigated previously. In the present study, we synthesize a series of

* Corresponding author.
E-mail address: runt@matse.psu.edu (J. Runt).

0032-3861/$ – see front matter © 2010 Elsevier Ltd. All rights reserved.
doi:10.1016/j.polymer.2010.07.030

segmented polyurethanes (with varying hard segment content) from MDI, BDO and the α,ω-bis(6-hydroxyethoxypropyl) PDMS macrodiol [24], and explore the phase-separated morphology, thermal properties, and unlike segment demixing.

2. Experimental

2.1. Materials

The polyurethanes used in the present study were synthesized using 4,4′-methylenediphenyl diisocyanate and 1,4-butanediol as the hard segment, and an α,ω-bis(6-hydroxyethoxypropyl) PDMS macrodiol as the soft segment (see Fig. 1). MDI and BDO were purchased from Sigma Aldrich (98% purity) and the α,ω-hydroxy-terminated PDMS was synthesized at AorTech Biomaterials. The hydroxyterminated poly(dimethylsiloxane) was subjected to thorough fractional distillation on a thin film evaporator and the distilled material was evaluated using gas chromatography to ensure that all low molecular weight cyclics were removed. Its number average molecular weight was determined to be 950 g/mol from end group analysis using nuclear magnetic resonance. The polydispersity index of the macrodiol was ~1.5 and the purity was greater than 97%.

The polyurethane copolymers were synthesized by a two-step bulk polymerization [24]. A prepolymer was prepared by addition of the macrodiol to a reaction vessel containing the MDI, and BDO was subsequently added for chain extension. Hard segment content was systematically varied from 26 to 52 wt%. These polymers are designated as *10026*, *10028*, *10030*, *10035*, *10040*, *10045* and *10052*; the first three digits (*100*) represent the fact that only the α,ω-bis(6-hydroxyethoxypropyl) PDMS was used as the macrodiol in these copolymers, and the last two digits correspond to the weight fraction of hard segments. The number average molecular weights of the synthesized copolymers ranged from 86 000 to 1 69 000 g/mol with a polydispersity of 1.6–2.1, as measured by gel permeation chromatography relative to polystyrene standards and using dimethylformamide (DMF) as the mobile phase.

120–140 μm thick films were cast from a solution of the polymers in N,N-dimethylacetamide (DMAc, Biolab Australia, minimum 99% purity) and heated at 55 °C for 16–18 h. The cast films were further dried under vacuum at 40 °C for another 24 h. Specimens then were retained at room temperature for about one month before characterization. All characterization was conducted on these specimens as-prepared, except for FTIR spectroscopy which required further solution casting.

2.2. Tapping mode atomic force microscopy (AFM)

Free film surfaces were scanned using a DI multimode AFM in tapping mode. Variable tapping forces were used in the experiments [r_{sp} = 0.3–0.8, where $r_{sp} = A/A_0$(the set point amplitude/the free amplitude of tip oscillation)] and the free amplitude was set to be 20 nm.

2.3. Transmission fourier transform infrared spectroscopy (FTIR)

Transmission FTIR spectroscopy was conducted using a Nicolet 6700 FTIR (Thermo Scientific). The polyurethane films described in Section 2.1 were dissolved in THF to create 2 wt% solutions. The solutions were cast onto KBr windows and dried overnight at 80 °C. Each sample was scanned 100 times at a resolution of 2 cm^{-1}.

2.4. Wide-angle X-ray diffraction (WAXD)

Wide-angle X-ray diffraction patterns were collected on a Rigaku DMAX/rapid micro-diffractometer in transmission mode using a copper point focused source (1.54 Å) at 50 kV and 40 mA.

2.5. Dynamic mechanical analysis (DMA)

Dynamic mechanical analysis was performed using a TA-Q800 DMA. DMA measurements were conducted at the heating rate of 3 °C/min and the frequency of 1 Hz in the tensile film mode.

2.6. Differential scanning calorimetry (DSC)

DSC measurements were performed on a TA-Q1000 DSC. Samples were first heated from −100 °C to 250 °C at a rate of 10 °C/min, rapidly cooled from 250 °C to −100 °C (within several minutes), then reheated from −100 °C to 250 °C at 10 °C/min.

2.7. Small-angle X-ray scattering (SAXS)

SAXS data were collected using a Molecular Metrology SAXS instrument with a CuKα radiation source ($\lambda = 0.154$ nm) and a two-dimensional multi-wire detector with the sample-to-detector distance of 1.5 m. Absolute scattered intensities were calculated by comparing the spectra of the samples to that of a pre-calibrated crosslinked polyethylene (S-2907) secondary standard [25].

3. Results and discussion

3.1. Nanoscale segregation

Tapping mode phase images of two representative PU copolymer films (*10035* and *10052* at a tapping force corresponding to r_{sp} = 0.3) are displayed in Fig. 2. As determined in prior investigations, the brighter regions (yellow) represent hard domains and the darker regions (brown) the soft segment–rich matrix. The hard

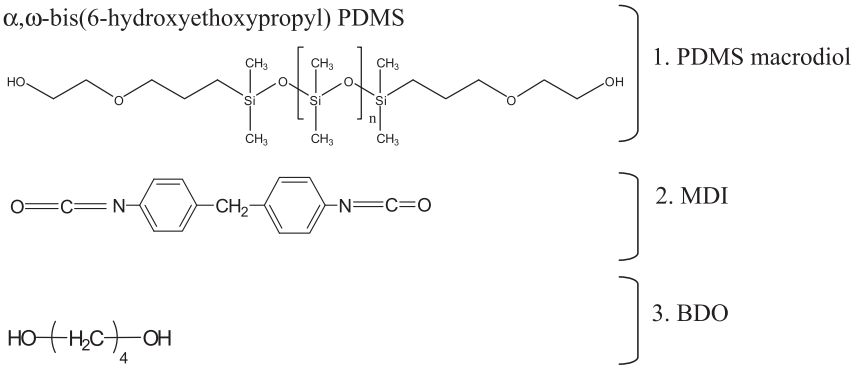

Fig. 1. Chemical structures of the components of the PDMS-based polyurethanes.

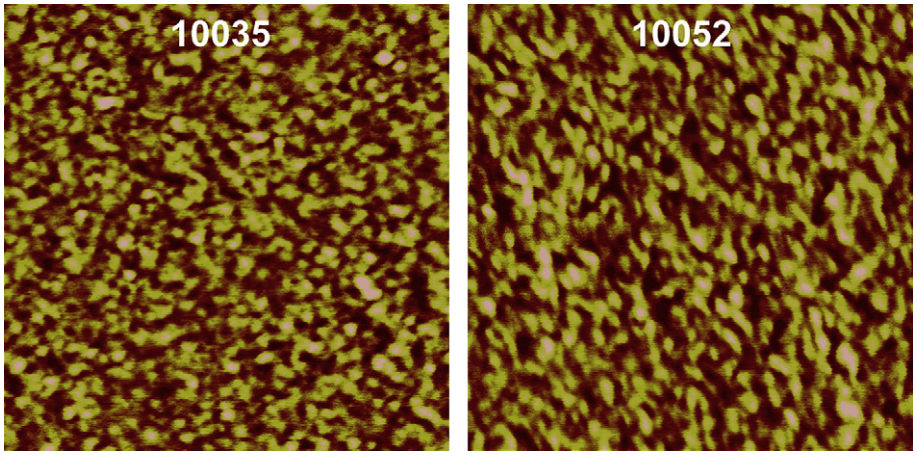

Fig. 2. Representative AFM tapping mode phase images of PDMS-PU surfaces (*10 035* and *10 052* at $r_{sp} = 0.3$). Scan size = 500 nm × 500 nm, scale = 20°.

domains are dispersed and are ~10 nm in diameter, and we do not observe any measurable differences between the morphologies of the various PDMS-based PUs under investigation here. One general finding is that as hard segment content increases, there is greater contrast between the microphases, but degrees of hard–soft segment demixing cannot be addressed from these images. The phase images of *10026–10052* also demonstrate that the hard domains are not very elongated [20,21,26], similar to our previous observations on other PDMS-based PUs [20,26], but in contrast to some other tapping mode AFM investigations of polyurethanes or poly(urethaneurea)s in which highly elongated or even continuous hard phases have been reported [27–29].

3.2. Hydrogen bonding from FTIR spectroscopy

Transmission FTIR spectroscopy was conducted on the *10026–10052* copolymers to investigate local hard segment organization by analyzing the state of hydrogen bonding of the urethane carbonyl groups. Since hydrogen bonds can only form in these copolymers between urethane carbonyls and N–H groups in other hard segments, a larger fraction of hydrogen-bonded carbonyls is expected to correlate with increasing hard segment segregation into hard domains [29,30]. All spectra were normalized by hard segment content by using the absorbance of the 3325 cm^{-1} N–H band (A_{3325}). Each spectrum is then divided by A_{3325} and scaled by hard segment content. With this normalization, the fraction of H-bonding among the copolymers can be readily compared.

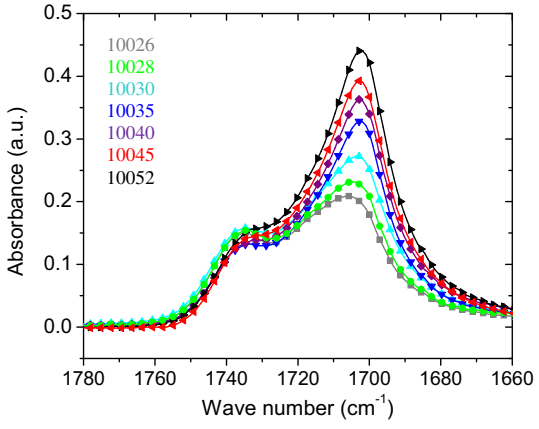

Fig. 3. FTIR spectra in the C=O stretching region from 1660 to 1780 cm^{-1}: (■) 10026; (●)10028; (▲) 10030; (▼) 10035; (◆) 10040; (◀) 10045; (▶) 10052. The spectra in this figure are scaled relative to the N–H absorbance at 3325 cm^{-1} and hard segment content of the copolymers.

The carbonyl regions of the FTIR spectra (1650–1780 cm^{-1}) of the *10026–10052* copolymers are displayed in Fig. 3. As established in previous studies [20,31], there are three bands in this region: assigned to strongly hydrogen-bonded carbonyl groups near 1703 cm^{-1}, loosely bonded hydrogen-bonded carbonyls near 1714 cm^{-1} and free (non-hydrogen-bonded) carbonyl groups near 1737 cm^{-1}. This spectral region was fit with three Gaussian–Lorentzian functions, and an iterative least-squares program was used to obtain the best fit of the experimental data by varying the frequency, width at half height and intensity of the three bands. The curve resolving results for the relative fractions of the three C=O environments are summarized in Table 1. The fraction of strongly H-bonded carbonyls increases significantly with increasing hard segment content. At the same time, the fractions of free carbonyls decrease significantly and the loosely bonded C=Os exhibit a small decrease with increasing hard segment content. This behavior is indicative of a considerable decrease in unlike segment mixing: the longer hard segment sequences in the higher hard segment content copolymers (formed due to the statistical nature of the polymerization) are less soluble with the ether end group segments of the soft segments (see Section 3.3.2), and are more strongly segregated as copolymer hard segment content increases. Although these findings are entirely consistent with the degrees of phase separation derived from SAXS experiments (see Section 3.4), we do not quantitatively compare the values from SAXS and FTIR: as noted earlier, the films used in our FTIR experiments were redissolved versions of the as-prepared films used in the remainder of our experiments. They are relatively thin and although were nominally provided with the same thermal history as the as-prepared films, their behavior may not be completely representative of the as-prepared materials.

Table 1
Curve fitting results in the carbonyl region of the FTIR spectra of *10026–10052*.

	Fraction of C=O groups		
	1737 cm^{-1}	1714 cm^{-1}	1703 cm^{-1}
10026	0.36	0.17	0.47
10028	0.32	0.13	0.55
10030	0.29	0.15	0.57
10035	0.28	0.13	0.59
10040	0.19	0.14	0.67
10045	0.18	0.14	0.68
10052	0.18	0.12	0.70

3.3. Phase transitions and crystallinity

3.3.1. Wide-angle X-ray diffraction

X-ray diffraction profiles of the various copolymers are displayed in Fig. 4. For all copolymers we observe two amorphous halos: at $2\theta = 12^\circ$ arising from phase-separated PDMS segments and at $2\theta = 20^\circ$ arising from non-PDMS segments [19,20]. In our earlier work on PDMS-based PUs there was no evidence of hard segment crystallinity from WAXD experiments, regardless of hard segment content [30,32]. However, the diffraction profiles of *10 040*, *10 045* and *10 052* exhibit weak diffraction peaks at 19° and 22.5° 2θ, corresponding to lattice spacings of 4.67 Å and 3.95 Å, respectively, in good agreement with the diffraction from MDI–BDO crystals [32,33]. The crystallinity of the current copolymers is clearly facilitated by the strong segregation between PDMS and MDI–BDO segments.

3.3.2. DMA

In Fig. 5, the storage moduli and mechanical tan δ for the *10026–10052* copolymers are presented. Storage moduli (Fig. 5(a)) increase with increasing hard segment content in the temperature range from −80 to −20 °C (i.e., at temperatures above the α relaxation of the PDMS phase). For all copolymers, the modulus decreases dramatically after passing through a second dynamic relaxation, $T_{\alpha 2}$, the origin of which is discussed below.

The dynamic relaxations are more evident in the tan δ plots in Fig. 5(b). The lowest temperature process, $T_{\alpha 1}$, arises from a phase composed predominately (or perhaps completely) of PDMS segments. The temperature location of α_1 does not change significantly with copolymer composition and the relaxation strength decreases with increasing hard segment content, as expected due to the reduced concentration of PDMS in the copolymers. Even though the degree of polymerization of the dimethylsiloxane units in the α,ω-bis(6-hydroxyethoxypropyl) PDMS is relatively small (~11 dimethylsiloxane repeat units), the strong chemical dissimilarity between the PDMS segments and the remainder of the segments in the copolymers drives segment demixing. In contrast to the PU copolymers investigated by Sheth et al. [34], the 950 g/mol PDMS segments in the present work are strongly segregated from the other components.

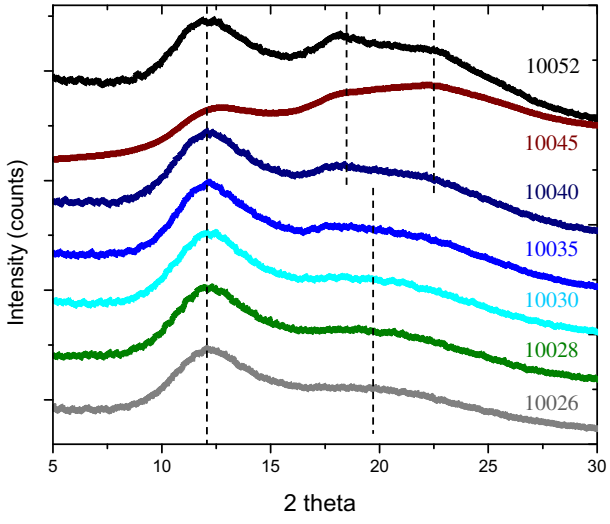

Fig. 4. WAXD patterns for *10026* (bottom) through *10052* (top) displaying two amorphous halos for PDMS segments and non-PDMS segments, and weak halos from crystallinity of PUs with high hard segment concentration.

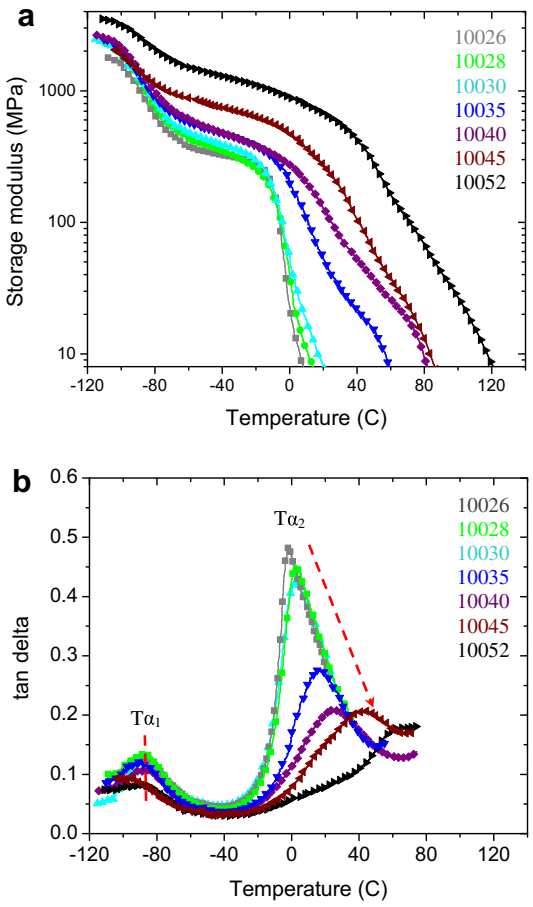

Fig. 5. (a) DMA storage modulus vs. temperature at 1 Hz and (b) the corresponding tan δ plot illustrating dynamic relaxation of microphase separated microstructure: (■) 10026; (●) 10028; (▲) 10030; (▼) 10035; (◆) 10040; (◀) 10045; (▶) 10052.

$T_{\alpha 2}$ has been shown previously to be associated with the segmental relaxation of a *mixed soft phase* consisting of PDMS end group segments and some dissolved hard segments [19,20]. [The α,ω-hydroxy-terminated PDMS macrodiol used in our experiments itself exhibits two T_gs, with the ether end group segments displaying a $T_g \sim -8$ °C.[20]] The temperature of α_2 relaxation increases from 0 to 50 °C with increasing copolymer hard segment content, while the strength of the relaxation decreases. The reduced α_2 relaxation strength arises from fewer ether end group segments available to participate in the mixed phase, as well as a smaller fraction of hard segments involved in the mixed phase. The latter arises because the average hard segment length in these copolymers increases with hard segment content [21] [for example, the fraction of 'lone' (single) MDIs between adjacent soft segments, relative to the total number of segments, decreases from 0.54 for *10026* to 0.04 for *10052*.] and longer hard segments are less soluble with ether end group segments from an entropy of mixing standpoint. The precise origin of the increase in $T_{\alpha 2}$ as hard segment content increases is less clear, since the fraction of hard segments in solution with the ether end group segments is unknown. As hard segment content increases, PDMS ether end group segments have a higher probability of attachment to longer hard segments, which in turn are more likely to reside in immobile hard domains, resulting in restricted end group segment mobility. Finally, a hard domain α relaxation is not observed in our experiments due to their termination at ~75 °C and below, due to their lack of overall stiffness.

3.3.3. DSC

DSC traces for segmented PU copolymers are well known to be rather complex, and there has been continued discussion throughout the past decades regarding the origin of the various thermal events observed [13,30,35–38]. Fig. 6 displays the DSC thermograms from the first heating of the ethoxypropyl PDMS copolymers having the same thermal history as the specimens explored in our other experiments. A T_g is observed below room temperature, increasing in temperature (from −15 to 18 °C) and decreasing in magnitude with increasing hard segment content. This is consistent with a similar change in $T_{\alpha 2}$ in the DMA experiments and so clearly corresponds to the T_g of the mixed phase. The T_g of the siloxane phase (−105 °C) [20] was not detected in these DSC measurements due to the lower limit of the testing temperature.

Two relatively small thermal events are observed in the 50–120 °C temperature range. The lower T process resides at ~60 °C regardless of copolymer composition, while that at higher T occurs near 80 °C for *10026*, perhaps increases in temperature slightly through *10045*, and is observed at ~110 °C for *10052*. The T_g of the high molecular weight MDI–BDO polymer is 110 °C [39] but hard segment sequence lengths in our ethoxypropyl PDMS copolymers are generally rather short due to the statistical nature of the polymerization, and T_g is well known to be a function of molecular weight, particularly at low degrees of polymerization. It stands to reason then that one of the events in this temperature range is associated with the hard domain T_g. Although both events appear as peaks as opposed to a simple change in heat capacity, it is well known that endotherms can accompany the heat capacity change at T_g of polymer glasses, arising from excess enthalpy contributions [40]. Our earlier SAXS temperature studies of ethoxypropyl PDMS soft segment PUs containing 20% PHMO [41] and similar preliminary experiments on *10040* [42], demonstrate that the SAXS invariant begins to gradually decrease above ~80 °C for both 40 wt % hard segment copolymers. For significant dissolution of the hard domains to proceed (see below), hard segments in hard domains must have sufficient mobility. Consequently, the transition at 80 °C is assigned to the T_g of the hard domains. The slight increase in hard domain T_g with increasing copolymer hard segment content is consistent with the longer mean hard segment lengths, but the origin of the abrupt increase for *10052* is unclear. Nevertheless, the process near 110 °C for *10052* remains in the feasible range of hard domain T_g.

What then is the origin of the process at ~60 °C? Recall that all samples were annealed at 55 °C for 16–18 h and further annealed under vacuum at 40 °C for another 24 h prior to DSC experiments, and it seems likely that the 60 °C endotherm is associated with this thermal history. An endotherm in this temperature range has been observed for other PU copolymers and been proposed to arise from ordering of 'lone' MDIs [13]. However, it is unclear what the driving force for such a process would be, particularly since 'lone' MDIs are dispersed in the mixed phase. Another proposal is that this process is associated with the disruption of domains with limited short-range order [36]. This assignment is generally supported but our recent temperature dependent SAXS measurements of ethoxypropyl PDMS soft segment PUs containing 20% PHMO, for which a small increase in mean interdomain spacing occurs in this temperature range [41].

A third endotherm first appears as a shoulder near 100 °C for *10026*, and moves progressively to higher temperatures with increasing hard segment content. Since only *10040–10052* display crystallinity, this endotherm is not associated with crystal melting. A more likely explanation is that this transition is associated with microphase mixing (i.e., dissolution of hard domains with the other segments). In the preliminary temperature dependent SAXS experiments on *10040* alluded to earlier, we observed that the SAXS scattering maximum due to microphase separation disappeared around 180–200 °C [42], near the conclusion of *10040*'s higher temperature endotherm (although crystal melting is superimposed for *10040–10052*, see below). This behavior is quite similar to that of a related PDMS-based copolymer investigated in one of our earlier publications [26]. Even though PDMS segments are strongly segregated at lower temperatures (driven by the chemical dissimilarity of the PDMS and hard segments as well as inter hard segment H-bonding), entropy of mixing dominates at elevated temperatures over unfavorable enthalpic contributions and equation of state effects, the former favored at higher temperatures since the PDMS and mean hard segment sequence lengths are relatively short. As we established in similar temperature dependent SAXS experiments,

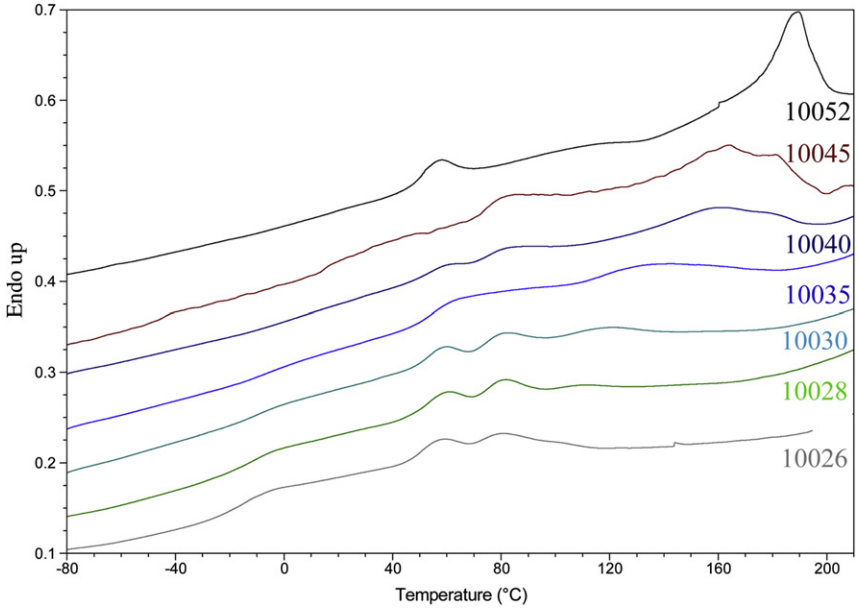

Fig. 6. DSC thermograms of PDMS-PU copolymers from first heating showing the glass transition temperatures and microphase mixing temperatures.

microphase mixing logically takes places at lower temperatures for lower hard segment content copolymers due to lower mean hard segment length. For example, the conclusion of the mixing process for ethoxypropyl PDMS soft segment PUs containing 20% PHMO varies significantly: from ~120 °C to ~ 200 °C for copolymers having 30–52 wt% hard segments [42]. By analogy, we therefore propose that the third DSC endotherm in the copolymers under investigation here arises from hard domain (segment) mixing with the other components.

Finally, as noted earlier in Section 3.3.1, copolymers *10040–10052* exhibit some hard domain crystallinity. This is in keeping with the observation of a fourth endotherm for *10040* (a shoulder appearing ~180 °C), which moves to progressively higher temperatures for *10045* and *10052*.

3.4. Degrees of unlike segment demixing

The background corrected SAXS scattering patterns of *10026–10052* are displayed in Fig. 7 in a plot of scattering intensity ($I(q)$) against scattering vector (q). The peak maxima (q_{max}) are related to the mean spacing between hard domains (d), $d = 2\pi/q_{max}$ and these are summarized in Table 2. For traditional two phase PUs, degrees of microphase separation can be determined from the ratio of the experimentally measured electron density variance (related to the total scattering intensity in absolute units) to the theoretical electron density variance (i.e., calculated for the hypothetical case of complete phase separation) [$\overline{\Delta\eta^{2\prime}}/\overline{\Delta\eta_c^2}$] [43,44]. The experimental electron density variance ($\overline{\Delta\eta^{2\prime}}$) is determined from the background corrected SAXS data [20]:

$$\overline{\Delta\eta^{2\prime}} = cQ = c\int \{I(q) - I_b(q)\}q^2 dq \tag{1}$$

where Q is the invariant and the constant c is

$$c = \frac{1}{2\pi^2 i_e N_{av}^2} = 1.76\times 10^{-24}\ \left(\text{mol}^2/\text{cm}^2\right) \tag{2}$$

The symbol i_e refers to Thompson's constant for the scattering from one electron (7.94×10^{-26} cm^2) and N_{av} is Avogadro's number. The measured electron density variances ($\overline{\Delta\eta^{2\prime}}$) are listed in Table 2. The *hypothetical* electron density variances for a two phase system ($\overline{\Delta\eta_c}$) are calculated assuming complete phase separation and sharp boundaries between hard and soft segment domains, and is defined as [45]:

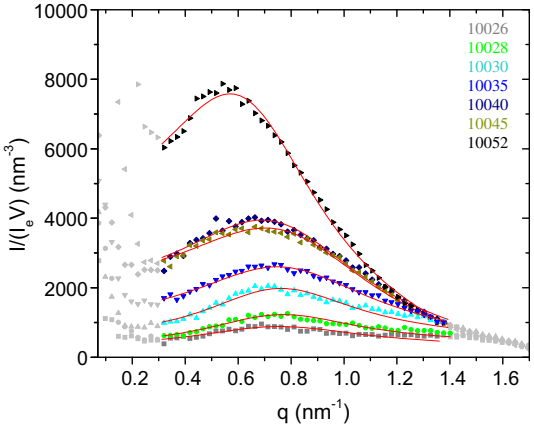

Fig. 7. Background corrected SAXS intensities and the fitting curves (red) by core-shell model of (■) 10026; (●) 10028; (▲) 10030; (▼) 10035; (◆) 10040; (◀) 10045; (▶) 10052. The light gray data points were not included in the fitting.

Table 2
Interdomain spacing, experimental electron density variances ($\overline{\Delta\eta^{2\prime}}$), theoretical electron density variances ($\overline{\Delta\eta_c^2}$) for hypothetical complete phase separation, and degrees of phase separation from $\overline{\Delta\eta^{2\prime}}/\overline{\Delta\eta_c^2}$ in the pseudo two-phase model.

	d (nm)	$\overline{\Delta\eta^{2\prime}} = cQ \times 10^3$ (mol e$^-$/cm^3)^2	$\overline{\Delta\eta_c^2} \times 10^3$ (HS/rest)	Degree of microphase separation
10026	9.2	0.38	1.86	0.20
10028	8.4	0.61	2.39	0.26
10030	9.2	1.12	2.84	0.39
10035	8.9	1.67	3.65	0.46
10040	9.5	2.16	4.19	0.52
10045	9.6	2.09	4.60	0.45
10052	11.3	3.10	4.75	0.65

$$\overline{\Delta\eta_c} = \phi_{hs}\phi_{ss}(\eta_{hs} - \eta_{ss})^2 = \phi_{hs}(1-\phi_{hs})(\eta_{hs} - \eta_{ss})^2 \tag{3}$$

where ϕ_{hs} and $\phi_{ss}$are the volume fractions of hard segments and soft segments in hypothetical completely phase-separated copolymers, respectively, and η_{hs} and η_{ss} are the electron densities of completely segregated hard and soft phases, respectively. In all of our calculations of the hypothetical "completely demixed" cases, we assume that only 'lone' MDIs (i.e., one MDI without BDO chain extender) are dissolved in the ether mixed phase, and longer hard segments are involved only in the hard phase.

The three phase copolymers under investigation present a more complex scenario than the traditional two phase case. As we have done in earlier investigations on related PDMS-based PUs, we apply two models for the analysis of the experimental SAXS data: a pseudo two-phase approach [46,47] and a core-shell (Yarusso–Cooper) model [48–50].

3.4.1. Pseudo two-phase model

As noted above, the copolymers under consideration here consist of a unique three phase microstructure: a PDMS phase, hard domains composed of hard segments, and a mixed phase of PDMS ether end group segments and some dissolved hard segments. In this first approach, we simplify the estimation of the theoretical electron density variances of *10026–10052* by using a *pseudo two-phase model*. In order to justify applying a pseudo two-phase model to the copolymers under consideration here, we first calculated the hypothetical electron density (η_i) and the volume fraction (Φ_i) of the three phases, and compared the average electron density with that of each phase. The volume fraction of hard segments (obtained from a group contribution method) and the calculated electron densities are listed in Table 3, and the calculation details are described in refs [20,21]. Since the average electron densities (η_{avg}) are comparable to the electron densities of the siloxane phase (η_{PDMS}), it is a reasonable approximation to consider the PDMS phase and the mixed phase to be one soft phase for the purposes of this model. The electron density of this pseudo-mixed soft phase

Table 3
The volume fraction of hard segment (v_{hs},%) from the group contribution method, theoretical electron densities (η_i in the unit of (mol e−/cm^3)^2) and volume fractions (ϕ_i) for ith phases in the PU copolymers; i = "PDMS" for PDMS only, i = "hs" for hard segments only, i = "mixed" for PDMS ether end group segments and lone MDIs, and i = "ps" for the "pseudo soft" phase (i.e., including PDMS, the ether end groups and lone MDIs).

	v_{hs} (%)	η_{PDMS}	ϕ_{PDMS}	η_{hs}	ϕ_{hs}	η_{mixed}	ϕ_{mixed}	η_{avg}	η_{ps}
10026	20.0	0.569	0.619	0.735	0.095	0.638	0.264	0.590	0.588
10028	21.7	0.569	0.604	0.735	0.126	0.639	0.242	0.591	0.587
10030	23.4	0.569	0.589	0.734	0.154	0.640	0.223	0.591	0.586
10035	27.7	0.569	0.551	0.732	0.216	0.642	0.187	0.592	0.585
10040	32.2	0.569	0.513	0.730	0.272	0.643	0.159	0.593	0.584
10045	36.8	0.569	0.473	0.729	0.323	0.645	0.139	0.595	0.584
10052	43.6	0.569	0.417	0.725	0.390	0.647	0.116	0.595	0.584

(including PDMS segments, ether end group segments and lone MDIs) is designated as η_{ps} in Table 3. *The hard domains (composed only of hard segments)* and *a soft phase containing the remainder of the segments (+lone MDIs)* are the two components considered in the pseudo two-phase model.

Applying this model to the ethoxypropyl PDMS soft segment copolymers, the degrees of phase separation indicate *what fraction of hard segments are not mixed in the pseudo-mixed soft phase*, with the remainder residing in the pseudo soft phase. As displayed in Table 2, the degrees of phase separation increase from 0.2 to 0.65 as copolymer hard segment content increases, in keeping with the general findings from FTIR experiments. The greater the fraction of hard segments in the copolymers, the longer the average hard segment length, and the larger the fraction of hard segments that phase separate together with other hard segments, rather than mixing with ether end group segments in the soft phase.

3.4.2. Core-shell model

The second model used for analyzing our experimental SAXS data is the core-shell (Yarusso–Cooper) model, which is a modified hard-sphere scattering model originally employed to analyze the scattering from ionomers [51]. We have shown previously that this model is applicable to similar PU segmented block copolymers containing PDMS-based soft segments [20,21], and expect it to be suitable in the present case as well. The schematic representation of proposed core-shell model is provided in Fig. 8, which displays the three phase organization of the copolymers under consideration.

The core-shell model is applied by fitting the experimental scattering curves with [20,50]:

$$I(q) = I_e(q)V\frac{1}{V_p}\Delta\eta_1^2\cdot V_1^2\Phi^2(qR_1)\frac{1}{1+(8V_{ca}/V_p)\cdot\varepsilon\cdot\Phi(2qR_{ca})} \quad (4)$$

where $I_e(q)$ is the intensity scattered by a single electron, V is the volume of the sample illuminated by the x-ray beam, V_p is the average sample volume per particle, ε is a constant ~ 1, $V_{ca} = 4/3\pi\cdot R_{ca}^3$ of which $2R_{ca}$ is the closest approach distance between two domains (assumed to be spherical, a good first approximation considering the AFM images in Fig. 2). The difference in electron density ($\Delta\eta_1$) between the scattering particles and the surrounding matrix is determined in the fitting by

$$\Delta\eta_1 = \eta_1 - \eta_2 \quad (5)$$

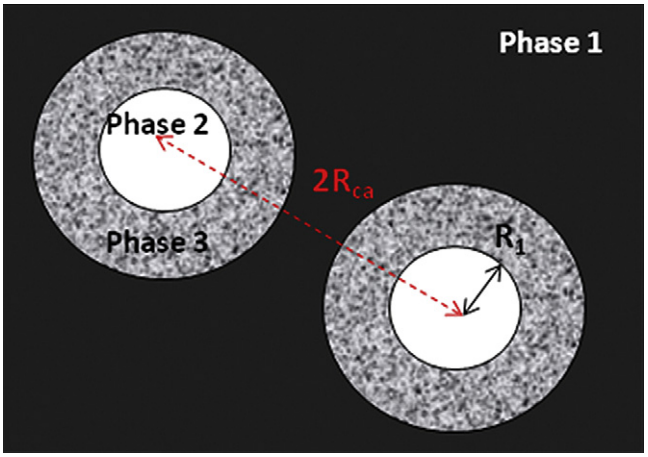

Fig. 8. Schematic of three phase organization of PDMS-PUs under consideration: Phase 1 = PDMS phase, Phase 2 = hard domains, Phase 3 = mixed phase of PDMS soft segment ether end group segments and some dissolved hard segments. $2R_{ca}$ = the closest approach distance between two hard domains and R_1 = the radius of a hard domain (scattering particle).

where phase 1 is composed of the siloxane units only (matrix) and phase 2 consists of the scattering particles (cores), and V_1 is the volume of a scattering core [20]. The other terms are defined as $\Phi(x) = 3\sin x - x\cos x/x^3$ and $V_1 = 4/3\pi\cdot R_1^3$, where R_1 (the radius of a scattering core) is smaller than R_{ca}.

The resulting fitted curves (red) are displayed with the experimental SAXS intensities in Fig. 7 [the fitted q range does not include the low q intensity upturn and the high q region [20]]. R_1, R_{ca}, and V_p in Table 4 were derived from the best fit of the model to the experimental data, and a nonlinear least-squares regression based on equation (4) was used to optimize the independent fitting parameters and generate the best-fit curves displayed in Fig. 7. Table 4 also lists the calculated differences in electron density, assuming complete phase separation of hard, siloxane and the mixed phases. The electron density difference between the siloxane matrix and the hard domain cores is:

$$\Delta\eta_{hs} = \eta_{hs} - \eta_1\ , \quad (6)$$

where *phase 1* is defined as the siloxane matrix and *phase hs* consists of the hard segments only. The difference in electron density between the siloxane matrix and the shell composed of PDMS end group segments and lone MDIs is:

$$\Delta\eta_m = \eta_m - \eta_1\ , \quad (7)$$

where *phase 1* is the siloxane matrix and *phase m* (for "mixed") is composed of the ether end segments of the PDMS soft segments and lone MDIs. These two values are calculated using the electron densities in Table 3 and the units are converted from molar quantities ($mol\cdot e^-/cm^3$) to atomic units (nm^{-3}).

In order to determine mean dimensions of the cores (hard domains) and shell (the mixed phase) from this model, the electron density difference ($\Delta\eta_1$) between the scattering particle and the matrix must be fixed to be the same as the calculated electron density difference ($\Delta\eta_{hs}$) between the hard domains and the siloxane matrix. However, as noted previously [20,26], for PDMS-based PUs containing more than 40% hard segments, the nonlinear least-squares regression provides adequate fits only when varying $\Delta\eta_1$ as a fitting parameter, and when the resulting $\Delta\eta_1$ lies between $\Delta\eta_{hs}$ as upper limit and $\Delta\eta_m$ as lower limit. In the case of varying $\Delta\eta_1$, we calculate the contribution of hard segments in the scattering particle (s_{hs}), by comparing the fitted electron density difference ($\Delta\eta_1$) with the two calculated electron density differences ($\Delta\eta_{hs}$ and $\Delta\eta_m$), using:

$$\Delta\eta_1 = s_{hs}\Delta\eta_{hs} + (1 - s_{hs})\Delta\eta_m \quad (8)$$

For ethoxypropyl PDMS soft segment copolymers with hard segment concentration of 35% and below, although the parameter s_{hs} is essentially fixed as equal to 1 by fixing $\Delta\eta_1 = \Delta\eta_{hs}$, it was

Table 4
Fitting parameters (noted as "fit") obtained from core-shell model, the calculated electron density differences, the size of the hard segment (noted as "cal").

	cal	cal	fit	fit	fit	fit	cal
	$\Delta\eta_{hs}$ (nm^{-3})	$\Delta\eta_m$ (nm^{-3})	$\Delta\eta_1$ (nm^{-3})	R_1 (nm)	R_{ca} (nm)	$V_p^{1/3}$ (nm)	s_{hs}
10026	99.9	41.8	99.9	1.3	3.5	10.0	1
10028	99.7	42.4	99.7	1.4	3.5	9.2	1
10030	99.4	43.0	99.4	1.5	3.5	9.2	1
10035	98.2	44.2	98.2	1.6	3.3	9.7	1
10040	96.9	44.5	84.8	1.9	3.4	10.2	0.77
10045	96.3	46.1	71.3	2.0	3.2	9.6	0.50
10052	93.9	46.8	91.3	2.3	4.0	12.4	0.94

allowed to float in the least-squares fitting routine and returned the expected value of 1, i.e., scattering particles are composed of only hard segments. R_1 was found to increase slightly with copolymer hard segment content and mean hard domain diameters ($2R_1$) of 3–4 nm were obtained. In all cases, the mean distance between hard domains is estimated as the cube root of the volume per scattering particle ($V_p^{1/3}$) and these fitted distances are close to the mean interdomain spacing (d) displayed in Table 2.

For ethoxypropyl PDMS copolymers with hard segment concentrations ≥40 wt%, $\Delta\eta_1$ was allowed to vary for optimal fitting and the corresponding s_{hs} was calculated (Table 4). $\Delta\eta_1$ values are slightly smaller than $\Delta\eta_{hs}$, and the scattering contributions of hard segments in *10040*, *10045* and *10052* are 0.77, 0.50 and 0.94, respectively. This indicates that some soft segments of low electron density are perhaps trapped in the hard domains, and the relative amount of trapped soft segments is smaller for *10052*. These results correspond well with the trend in the degree of microphase separation of these PUs with high hard segment content.

4. Summary

Segmented PUs with soft segments derived from α,ω-bis(6-hydroxyethoxypropyl) PDMS macrodiol were synthesized with varying hard segment contents, in order to investigate the microstructural organization of these unique copolymers. From the combined results from AFM, DMA and DSC experiments, these copolymers, like their mixed soft segment counterparts, were found to exhibit three microphases: a PDMS phase, hard domains, and a mixed phase containing PDMS ether end group segments and some dissolved hard segments. Findings from FTIR spectroscopy clearly show that the fraction of strongly hydrogen-bonded carbonyl groups, which arises from hard segment–hard segment interactions and therefore is a measure of hard segment segregation, increases with increasing hard segment content in the copolymers. Two models were applied to experimental SAXS data in order to additionally investigate degrees of microphase separation. Analysis with a pseudo two-phase model demonstrates that a greater fraction of hard segments become involved in hard domains, rather than being dissolved in the mixed phase, as hard segment content increases. In addition, using a core-shell model, we determined the mean size of the hard domain cores to be 3–4 nm for all copolymers and the interdomain distances from fitting correspond well with the experimental values. For ethoxypropyl PDMS copolymers with higher hard segment contents, the scattering contribution of the hard segments in the scattering particle was calculated and the trend in the fraction of hard segments involved in hard domains matches well with the degree of phase segregation derived from the pseudo two-phase model. The overall findings from the two SAXS models are in good qualitative agreement.

Acknowledgments

The authors would like to thank Amanda McDermott for her assistance with the WAXD experiments, Prof. Paul C. Painter for helpful discussions on FTIR spectra fitting, and Prof. Evangelos Manias for using his AFM.

References

[1] Ghanbari H, Viatge H, Kidane AG, Burriesci G, Tavakoli M, Seifalian AM. 2009; 27: 359–367.
[2] Lambda NMK, Woodhouse KA, Cooper SL. Polyurethanes in biomedical applications. Boca Raton: CRC Press; 1998.
[3] Yilgor I, McGrath JE. Adv Polym Sci 1988;86:1.
[4] Anderson JM, Hiltner A, Wiggins MJ, Schubert MA, Collier TO, Kao WJ, et al. Polym Int 1998;46:163–71.
[5] Christenson EM, Dadsetan M, Wiggins M, Anderson JM, Hiltner A. J Biomed Mater Res Part A 2004;69A:407–16.
[6] Christenson EM, Patel S, Anderson JM, Hiltner A. Biomaterials 2006;27: 3920–6.
[7] Ward R, Anderson J, McVenes R, Stokes KJ. Biomed Mater Res 2006;77A:580.
[8] Speckhard TA, Gibson PE, Cooper SL, Chang VSC, Kennedy JP. Polymer 1985;26:55–69.
[9] Brunette CM, Hsu SL, Rossman M, Macknight WJ, Schneider NS. Polym Eng Sci 1981;21:668–74.
[10] Tyagi D, Wilkes GL, Yilgor I, McGrath JE. Polym Bull 1982;8:543–50.
[11] Speckhard TA, Strate GV, Gibson PE, Cooper SL. Polym Eng Sci 1983;23: 337–49.
[12] Yu X-H, Nagarajan MR, Grasel TG, Gibson PE, Cooper SL. J Polym Sci Polym Phys Ed 1985;23:2319–38.
[13] Adhikari R, Gunatillake PA, McCarthy SJ, Meijs CF. J Appl Polym Sci 2000;78: 1071–82.
[14] Gunatillake PA, Meijs GF, McCarthy SJ, Adhikari R. J Appl Polym Sci 2000;76: 2026–40.
[15] Hsu SH, Tseng HJ. J Biomater Appl 2004;19:135–46.
[16] Martin DJ, Warren LAP, Gunatillake PA, McCarthy SJ, Meijs GF, Schindhelm K. Biomaterials 2000;21:1021–9.
[17] Simmons A, Hyvarinen J, Odell RA, Martin DJ, Gunatillake PA, Noble KR, et al. Biomaterials 2004;25:4887–900.
[18] Simmons A, Hyvarinen J, Poole-Warren L. Biomaterials 2006;27:4484–97.
[19] Choi T, Weksler J, Padsalgikar A, Runt J. Aust J Chem 2009;62:794–8.
[20] Hernandez R, Weksler J, Padsalgikar A, Runt J. Macromolecules 2007;40: 5441–9.
[21] Hernandez R, Weksler J, Padsalgikar A, Choi T, Angelo E, Lin JS, et al. Macromolecules 2008;41:9767–76.
[22] Meijs GF, Gunatillake PA, McCarthy SJ. US, 2001.
[23] Hernandez R, Weksler J, Padsalgikar A, Runt JJ. Biomed Mater Res 2008;87A: 546–56.
[24] Padsalgikar A. Australia, 2007 (US patent pending: filing number 60/744,097).
[25] Russell TP, Lin JS, Spooner S, Wignall GD. J Appl Crystallogr 1988;21:629–38.
[26] Choi T, Weksler J, Padsalgikar Ajay, Runt J. Polymer 2009;50:2320–7.
[27] Das S, Yilgor I, Yilgor E, Wilkes GL. Polymer 2008;49:174–9.
[28] Garrett JT, Siedlecki CA, Runt J. Macromolecules 2001;34:7066–70.
[29] Sheth JP, Wilkes GL, Fornof AR, Long TE, Yilgor I. Macromolecules 2005;38: 5681–5.
[30] Pukanszky B, Bagdi K, Tovolgyi Z, Varga J, Botz L, Hudak S, et al. Eur Polym J 2008;44:2431–8.
[31] Coleman MM, Lee KH, Skrovanek DJ, Painter PC. Macromolecules 1986;19: 2149–57.
[32] Blackwell J, Nagarajan MR, Hoitink TB. Polymer 1982;23:950–6.
[33] Koberstein JT, Galambos AF. Macromolecules 1992;25:5618–24.
[34] Sheth JP, Aneja A, Wilkes GL, Yilgor E, Atilla GE, Yilgor I, et al. Polymer 2004; 45:6919–32.
[35] Seymour RW, Cooper SL. 1971; 9: 689-&.
[36] Koberstein JT, Russell TR. Macromolecules 1986;19:714–20.
[37] Saiani A, Daunch WA, Verbeke H, Leenslag JW, Higgins JS. Macromolecules 2001;34:9059–68.
[38] Saiani A, Novak A, Rodier L, Eeckhaut G, Leenslag JW, Higgins JS. Macromolecules 2007;40:7252–62.
[39] Leung LM, Koberstein JT. Macromolecules 1986;19:706–13.
[40] Struik LCE. Physical aging in amorphous polymers and other materials. Amsterdam: Elsevier Scientific Pub. Co.; 1978.
[41] Pongkitwitoon S, Hernandez R, Weksler J, Padsalgikar A, Choi T, Runt J. Polymer 2009;50:6305–11.
[42] Pongkitwitoon S, Runt J. Unpublished results.
[43] Bonart R, Muller EH. J Macromol Sci Phys B 1974;10:177–89.
[44] Leung LM, Koberstein JT. J Polym Sci Polym Phys Ed 1985;23:1883–913.
[45] Tyagi D, McGrath JE, Wilkes GL. Polym Eng Sci 1986;26:1371–98.
[46] Wu W. Polym Bull 1982;23:1907–12.
[47] Koberstein JT, Stein RS. J Polym Sci Pt B-Polym Phys 1983;21:1439–72.
[48] Visser SA, Cooper SL. Macromolecules 1991;24:2584–93.
[49] Visser SA, Pruckmayr G, Cooper SL. Macromolecules 1991;24:6769–75.
[50] Yarusso DJ, Cooper SL. Macromolecules 1983;16:1871–80.
[51] Yarusso DJ, Cooper SL. Polymer 1985;26:371–8.